

Globally optimal volume-trap arrangements for the narrow-capture problem inside a unit sphere

Jason Gilbert* and Alexei Cheviakov†

Department of Mathematics and Statistics, University of Saskatchewan, Saskatoon S7N 5E6, Canada

 (Received 18 July 2018; revised manuscript received 21 November 2018; published 7 January 2019)

The determination of statistical characteristics for particles undergoing Brownian motion in constrained domains has multiple applications in various areas of research. This work presents an attempt to systematically compute globally optimal configurations of traps inside a three-dimensional domain that minimize the average of the mean first passage time (MFPT) for the narrow capture problem, the average time it takes a particle to be captured by any trap. For a given domain, the mean first passage time satisfies a linear Poisson problem with Dirichlet-Neumann boundary conditions. While no closed-form general solution of such problems is known, approximate asymptotic MFPT expressions for small traps in a unit sphere have been found. These solutions explicitly depend on trap parameters, including locations, through a pairwise potential function. After probing the applicability limits of asymptotic formulas through comparisons with numerical and available exact solutions of the narrow capture problem, full three-dimensional global optimization was performed to find optimal trap positions in the unit sphere for $2 \leq N \leq 100$ identical traps. The interaction energy values and geometrical features of the putative optimal trap arrangements are presented.

DOI: [10.1103/PhysRevE.99.012109](https://doi.org/10.1103/PhysRevE.99.012109)

I. INTRODUCTION

First-passage problems concern the time $\tau(x)$ during which a particle undergoing Brownian motion will wander a domain before it encounters some absorbing boundary. The time required for such an encounter to occur, averaged over multiple runs starting from the same initial position x , is referred to as the mean first-passage time (MFPT) $v(x)$. This notion is used in various applications, including the diffusion of protein receptors [1], the interaction between proteins and DNA [2], predator-prey dynamics [3], and multiple other research areas (see, e.g., Refs. [4,5]).

For a bounded domain $\Omega \subset \mathbb{R}^n$, $n = 2, 3$, with absorbing traps and an otherwise reflecting boundary, the MFPT is known to satisfy a Poisson problem with strongly heterogeneous Dirichlet-Neumann boundary conditions (cf. Refs. [6,7]), given by

$$\Delta v(x) = -\frac{1}{D}, \quad x \in \Omega \setminus \Omega_a, \quad (1.1a)$$

$$\partial_n v = 0, \quad x \in \partial\Omega, \quad v = 0, \quad x \in \partial\Omega_a = \bigcup_{j=1}^N \partial\Omega_{\epsilon_j}, \quad (1.1b)$$

where Δ is the Laplacian operator, D is the diffusivity of the Brownian motion, $\Omega_a \subset \Omega$ is the set of absorbing traps, $\partial_n v$ denotes the normal derivative on the surface $\partial\Omega$ of Ω , and $\partial\Omega_{\epsilon_j}$ is the surface of a trap. The average mean first-passage time (AMFPT) is defined as

$$\bar{v} = \frac{1}{|\Omega|} \int_{\Omega} v(x) d^n x, \quad (1.2)$$

where $|\Omega|$ is the measure, volume or area, of the domain. In the study of random walks, the average mean first-passage time is also known as the global mean first-passage time (GMFPT) [8,9]. [A similar boundary value problem (BVP) for the Laplace equation in two dimensions is known as the *Keldysh-Sedov problem* (see, e.g., Refs. [10,11]).]

In this work we consider the narrow capture problem in a three-dimensional spherical domain. The narrow capture problem is a first-passage problem characterized by the presence of localized absorbing traps within the domain, where the volume occupied by the traps is asymptotically small in some parameter. A schematic of the problem is shown in Fig. 1. The narrow capture problem has applications in the modeling of biophysical phenomena [12], simple particle reactions [7], and solid state physics [13,14]. For recent results on the narrow capture problem, see Refs. [15–18].

In addition to the biological interpretation of the problem, it is known that many first-passage problems can be considered from the perspective of electrostatics [7]. The MFPT problem (1.1) is identical to that of an electrostatics problem in which $v(x)$ describes the electric potential within a domain which contains an electric field like that which would be created by a uniform charge distribution. The boundary conditions at the domain boundary correspond to the existence of a field which, at the spherical boundary, exactly cancels the component of the internal electric field which is normal to the surface; the boundary conditions on the trap surfaces mean they could be interpreted as perfect conductors. The electrical confinement of particles is a wide field of study [19–22], which includes the study of arrangements of small metallic particles in a container [23], a situation which bears some resemblance to the narrow capture problem considered in this work.

Except for the very simplest cases, exact explicit solutions of the narrow capture problem (1.1) are not known. In order to compute the MFPT $v(x)$ and/or the AMFPT \bar{v} in a generic

*Corresponding author: jtg074@mail.usask.ca

†Alternative English spelling: Alexey Shevyakov; shevyakov@math.usask.ca

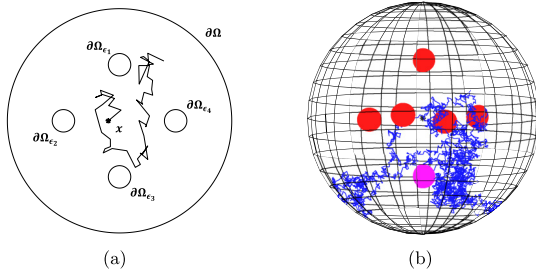


FIG. 1. (a) A two-dimensional narrow capture problem in the unit disk having internal traps with absorbing boundaries $\{\partial\Omega_{\epsilon_j}\}$. (b) A three-dimensional narrow capture problem, a sample Brownian particle trajectory, leading to a capture in a trap (lowermost) denoted by purple.

domain with volume traps, one has to either retreat to a full numerical solution of (1.1) or perform computations using simulated Brownian motion starting from a given point of the domain. Such computations are computationally expensive and, moreover, do not provide explicit information about the structure of the problem, such as the dependence of MFPT and AMFPT on trap locations in the domain Ω , on trap sizes, orientations, etc.; in order to study such dependencies, the problem (1.1) would require a new numerical solution for each infinitesimal configuration change. In particular, “global” questions, such as the calculation of optimal trap positions in a given domain that would minimize MFPT (AMFPT), can be addressed only if some kind of an explicit formula for the MFPT is known.

Recent work on the narrow capture problem [24] used matched asymptotic expansions to derive an explicit approximation for the MFPT $v(x)$ and the AMFPT \bar{v} for N small, well-separated traps in the unit sphere (Sec. II). In addition to depending on the trap information (size, number, and shape information through the capacitance coefficient), these asymptotic formulas depend on trap positions through the terms involving the Neumann Green’s function of the Poisson problem. This provides a handle to examine the relationship between, for example, the average MFPT for the Brownian particles traveling in the spherical domain and the geometry of the trap arrangement.

The main objective of this paper is the study of optimal configurations of traps within the unit sphere, that is, the arrangements of the traps that minimize the AMFPT. In the context of the narrow capture problem, such an arrangement of traps can be thought of as the one which, on average, most quickly captures particles wandering the domain, regardless of their initial position. In terms of the analogous electrostatic problem, this optimum would be the distribution of N small conductors which minimizes the electric potential per unit volume. In particular, we test a previously expressed conjecture that the optimal configurations might have the traps distributed over spherical surfaces nested within the unit sphere physical domain. In order to study such optimal trap arrangements, the asymptotic MFPT approximations of Ref. [24] are employed. Similar work has been done for narrow capture problems in two dimensions [25], as well as the closely related *narrow escape* problem, which considers

an absorbing set which contains asymptotically small areas of the boundary of the domain [26–30]. The optimal placement of such an absorbing set can be thought of as one which maximizes the rate at which some diffusion through the boundary of the domain occurs.

The current contribution is organized as follows. In Sec. II we review the MFPT and AMFPT approximation formulas for the case of N small well-separated traps of size $\epsilon \ll 1$ [24], as well as the exact solution for a finite single spherical trap centered at the origin of the domain. For the asymptotic N -trap solution, the leading term depends only on the “total amount” of traps, and the second-order term involves a pairwise quantity depending on the trap arrangement.

In Sec. III the exact and finite-element numerical solutions of the MFPT problem (1.1) are employed to examine the accuracy and applicability limits of the asymptotic MFPT approximations throughout the domain, as functions of location, trap proximity, trap sizes, and boundary effects. From test computations run for simple yet characteristic trap configurations, it is observed that the asymptotic MFPT approximations may remain applicable and accurate well beyond the limits in which they were derived. Similar observations have been previously made for narrow escape problems in two and three dimensions [28].

In Sec. IV we use the explicit AMFPT formulas and a Matlab interface for a global optimization software package [Lipschitz-continuous global optimization (LGO) [31]] to compute optimal AMFPT-minimizing configurations for N equal traps in a unit sphere, in the range $2 \leq N \leq 100$. A graph of the trap arrangement-dependent part of the AMFPT as a function of the trap number N is obtained, and a geometrical characterization of the computed putative optimal spherical volume trap arrangements is presented. The radial distributions of the traps in optimal configurations are studied; it is found that the traps are indeed distributed close to, though not exactly on, the surfaces of concentric spheres inside the spherical problem domain. Finally, a table of minimal values of trap interaction energies and the corresponding radial trap distributions are listed for optimal designs of $2 \leq N \leq 100$ traps. Global optimization problems for confined interacting particles arise in a wide variety of applications. Many papers consider such problems from theoretical and computational points of view, in various dimensions and domain geometry (see, e.g., Refs. [29,32–35] and references therein). One of the essential interesting and important features of global optimization problems involving pairwise potentials is the existence of local minima, the number of which quickly grows with N ; in particular, in some applications, those numbers are believed to increase exponentially [33,35]. Local and global minima of trap configurations interacting through a pairwise Coulombic, logarithmic, and power-law potentials have been studied in a recent work [36] (see also Refs. [32–34]). The work presented in the current contribution presents the first unconstrained three-dimensional computation of optimal volume trap configurations for the narrow capture problem (1.1), based on the pairwise potential provided by the explicit asymptotic MFPT solutions.

The final Sec. V includes a summary and discussion of the results and open problems.

II. THE ASYMPTOTIC SOLUTION OF THE NARROW CAPTURE PROBLEMS WITH MULTIPLE SMALL TRAPS IN A UNIT SPHERE

It is evident that the location of the traps within the physical domain, referred to here as the *trap configuration*, determines the boundary conditions of the MFPT problem (1.1), as the surfaces of the traps define the absorbing boundary conditions within the domain. Even for simple trap configurations, the linear problem (1.1) has no closed-form solution due to the complex geometry of boundary conditions provided by the trap surfaces. For the simplest configuration, the unit sphere domain with a single spherical trap of radius ϵ at the origin, the exact solution in spherical coordinates is readily found, given by

$$v_e(r) = \frac{1}{6D} \left[\frac{\epsilon^3 + 2}{\epsilon} - \frac{r^3 + 2}{r} \right], \quad (2.1a)$$

depending only on the distance r from the origin, and the corresponding AMFPT is given by

$$\bar{v}_e = \frac{1}{6D} \left[\frac{\epsilon^3 + 2}{\epsilon} - \frac{18}{5} \right]. \quad (2.1b)$$

For more complicated trap configurations, or nonspherical domains, exact solutions of the MFPT problem (1.1) are not available. Numerical approximations of (1.1) quickly become computationally intensive as the number of traps increase, particularly when traps of small sizes are considered, since many points must be sampled around each trap to obtain sufficient resolution. Following the work on a related problem with surface traps [27], in Ref. [24], explicit asymptotic solutions of the problem (1.1) for the unit sphere containing N small, well-separated, generally nonidentical traps were derived. It was shown that the leading-order terms of MFPT and AMFPT are given by

$$v_A(x) = \frac{|\Omega|}{4\pi N \bar{c} D \epsilon} \left[1 - 4\pi \epsilon \sum_{j=1}^N c_j G(x; x_j) + \frac{4\pi \epsilon}{N \bar{c}} p_c(\xi_1, \dots, \xi_N) + O(\epsilon^2) \right], \quad (2.2a)$$

$$\bar{v}_A = \frac{|\Omega|}{4\pi N \bar{c} D \epsilon} \left[1 + \frac{4\pi \epsilon}{N \bar{c}} p_c(x_1, \dots, x_N) + O(\epsilon^2) \right], \quad (2.2b)$$

where N is the number of traps of size $O(\epsilon)$, $\epsilon \ll 1$, x_j is the position vector of the j th trap, c_j is the *capacitance* of the j th trap (a quantity related to the shape of the trap), and $\bar{c} = \frac{1}{N} \sum_{j=1}^N c_j$ is the average capacitance. [For a single spherical trap of radius $a\epsilon$, the capacitance is given by $c = a\epsilon$. Capacitances for some other simple trap shapes are given in Table I. The capacitances c presented in the table are related with the classical electric capacitances of isolated electric conductors \tilde{c} : $\tilde{c} = 4\pi \epsilon c$, where ϵ is the dielectric permittivity of the material surrounding the conductor, and $\epsilon = 1$ for the vacuum.]

The leading-order term of the variable and the average asymptotic MFPTs $v_A(x)$, $\bar{v}_A \sim O(1/N\epsilon)$ in (2.2) is inversely proportional to the trap size ϵ and the trap number N ;

TABLE I. Capacitances c_j of some simple trap shapes [24,37,38].

| Trap shape | Capacitance |
|---|---|
| Sphere of radius $a\epsilon$ | $c_j = a\epsilon$ |
| Hemisphere of radius $a\epsilon$ | $c_j = 2a\epsilon(1 - \frac{1}{\sqrt{3}})$ |
| Flat disk of radius $a\epsilon$ | $c_j = \frac{2a\epsilon}{\pi}$ |
| Prolate spheroid with semimajor and semiminor axes $a\epsilon, b\epsilon$ | $c_j = \epsilon \frac{\sqrt{a^2 - b^2}}{\operatorname{arccosh}(a/b)}$ |
| Oblate spheroid with semimajor and semiminor axes $a\epsilon, b\epsilon$ | $c_j = \epsilon \frac{\sqrt{a^2 - b^2}}{\operatorname{arccos}(b/a)}$ |

the second-order terms depend on the spatial locations of the traps inside the domain through the Neumann Green's function $G(x; x_j)$ for the Laplacian and the pairwise ‘‘interaction energy’’ term p_c defined below. The approximate solutions (2.2) were derived using matched asymptotic expansions [24], in which the outer expansion of the solution in terms of a generalized power series in the small parameter ϵ , holding in a region away from an $O(\epsilon)$ neighborhood of a trap located at x_j , was matched to the inner solutions defined within an $O(\epsilon)$ region around the trap in terms of appropriately rescaled coordinates. The resulting leading-order matching conditions are solved to obtain the asymptotic MFPT expression (2.2a). We note that the AMFPT \bar{v}_A is related to the principal eigenvalue $\lambda(\epsilon)$ of a linear Laplacian eigenvalue problem [see Eq. (1.1) in Ref. [24]], with the same boundary conditions as in the MFPT problem (1.1): $\lambda(\epsilon) \sim 1/(D\bar{v})$.

The interaction energy term p_c is expressed through a sum of the Green's functions $G(x, \xi)$ computed on trap pairs and their regular parts $R(\xi)$ computed at single trap locations. For the unit sphere, G is known explicitly (see, e.g., Ref. [24] and references therein), while for more complicated domains, closed-form expressions of the Green's function are generally not available.

Defining

$$\begin{aligned} \Gamma(x; \xi) = G(x, \xi) &= \frac{1}{4\pi|x - \xi|} + \frac{1}{4\pi|x||x' - \xi|} \\ &+ \frac{1}{4\pi} \log \left(\frac{2}{1 - |x||\xi| \cos \theta + |x||x' - \xi|} \right) \\ &+ \frac{1}{8\pi} (|x|^2 + |\xi|^2) - \frac{7}{10\pi}, \end{aligned} \quad (2.3a)$$

$$\begin{aligned} \Gamma(\xi; \xi) = R(\xi) &= \frac{1}{4\pi(1 - |\xi|^2)} + \frac{1}{4\pi} \log \left(\frac{1}{1 - |\xi|^2} \right) \\ &+ \frac{|\xi|^2}{4\pi} - \frac{7}{10\pi}, \end{aligned} \quad (2.3b)$$

one has the following simple expression for the interaction energy:

$$p_c(\xi_1, \dots, \xi_N) = \sum_{i=1}^N \sum_{j=1}^N c_i c_j \Gamma(\xi_i, \xi_j); \quad (2.4)$$

specific details can be found in Ref. [24]. In (2.3), ξ and x are positions within the spherical domain, x' is a point symmetric

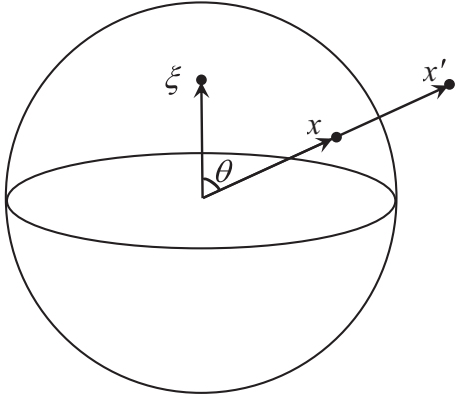


FIG. 2. Spatial components in (2.3).

to x with respect to the sphere: $|x||x'| = r^2 = 1$, and θ is the angle between the directions of ξ and x (Fig. 2).

The known terms of the asymptotic MFPT and AMFPT formulas (2.2) are explicit and can be readily used for computations. Moreover, due to their dependence on trap positions, one can use the asymptotic MFPT expressions to study *optimal trap arrangements* minimizing the AMFPT by optimizing the interaction term (2.4). Recently it has been found that these optimal arrangements correspond to an equilibrium configuration of localized spots in a singularly perturbed Schnakenberg reaction-diffusion model [39]. Such optimal arrangements are systematically sought in Sec. IV.

Though the asymptotic formulas (2.2) have been derived in the assumption of small well-separated traps, and provide MFPT estimates at the points x “far” from every trap, the practical applicability limits of these formulas may in fact be much wider. This is known to be the case, for example, for narrow escape problems with boundary traps [27,28,40]. In Sec. III we use exact and numerical solutions to study the quality of the asymptotic approximation (2.2) depending on the position of the point in the domain, distance between the traps, and the proximity of a trap to the domain boundary.

III. THE ACCURACY OF THE ASYMPTOTIC APPROXIMATION FOR THE SPHERICAL DOMAIN

In the limits of their validity, asymptotic approximate solutions such as (2.2) provide a powerful tool to study the narrow capture problem (1.1). Indeed, they are given by explicit formulas, which may be used for analysis and optimization, and also allow for straightforward computations of the approximate MFPT and AMFPT values, carried out quickly in comparison to full numerical simulations.

In the current section, we carry out some comparisons to obtain qualitative validity characteristics of the asymptotic MFPT approximations given by (2.2). In the derivation of the formulas (2.2), it was assumed that the total volume of the domain occupied by the traps was asymptotically “small” in ϵ , and also that the traps were “well separated” by distances much larger than the trap sizes. Another essential feature of the narrow capture problem (1.1) is the presence of a large reflecting boundary; one consequently expects that the

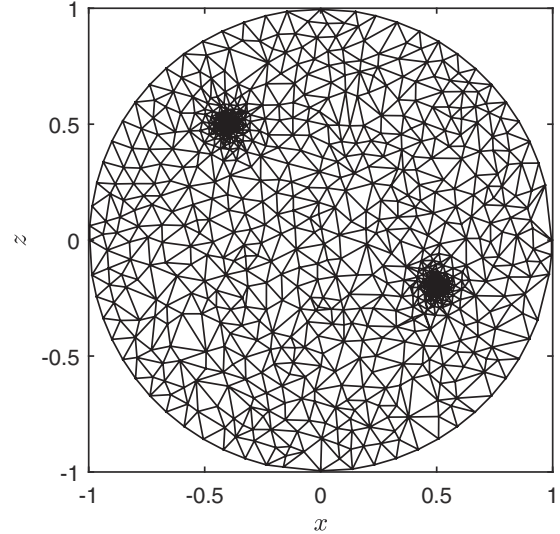


FIG. 3. An x - z projection view of a sample three-dimensional mesh slice from a COMSOL-based numerical MFPT computation: the case of a spherical domain containing five traps located at the Cartesian points $\xi_1 = (0.5, 0.1, -0.2)$, $\xi_2 = (0.3, 0.5, 0.1)$, $\xi_3 = (-0.4, 0.1, 0.5)$, $\xi_4 = (0.3, -0.3, 0.3)$, $\xi_5 = (-0.5, -0.3, -0.5)$. (The mesh points within $0.07 \leq y \leq 0.13$ are shown.)

asymptotic solution may not be precise when traps are located “close” to the spherical shell.

In order to estimate the effects of these assumptions on the accuracy of the approximation, we make comparisons of the asymptotic approximation (2.2) to the exact solution (2.1) for a single spherical trap located at the center of the domain, as well as to finite element-based numerical solutions for configurations with multiple traps. Let us define the relative errors of the MFPT and AMFPT as

$$\delta v(x) = \frac{|v_A - v|}{v}, \tag{3.1a}$$

$$\delta \bar{v} = \frac{|\bar{v}_A - \bar{v}|}{\bar{v}}, \tag{3.1b}$$

where $v_A = v_A(x)$ and \bar{v}_A are given by (2.2). In cases when $v(x)$, \bar{v} correspond to an exact solution, the quantities $\delta v(x)$ and $\delta \bar{v}$ (3.1) are the relative errors of the asymptotic approximation. When an exact solution is not available, the numerical solutions $v(x) = v_N(x)$ and $\bar{v} = \bar{v}_N = \text{const}$ will be used to illustrate the relative errors of the asymptotic formulas (2.2). In particular, we will examine the dependence of the error $\delta v(x)$ on the initial position x of the Brownian particles, the dependence of the AMFPT error $\delta \bar{v}$ on the relative positions of the traps, and the total volume occupied by the traps.

For trap configurations other than a single spherical trap centered at the origin, exact solutions of the volume narrow capture problem (1.1) do not appear in the literature. For the comparisons involving more complicated trap configurations, COMSOL Multiphysics software was used to obtain the numerical solutions of (1.1). In this finite-element solver, three-dimensional meshes refined around the trap boundaries were used. A sample mesh slice for a five-trap configuration is shown in Fig. 3.

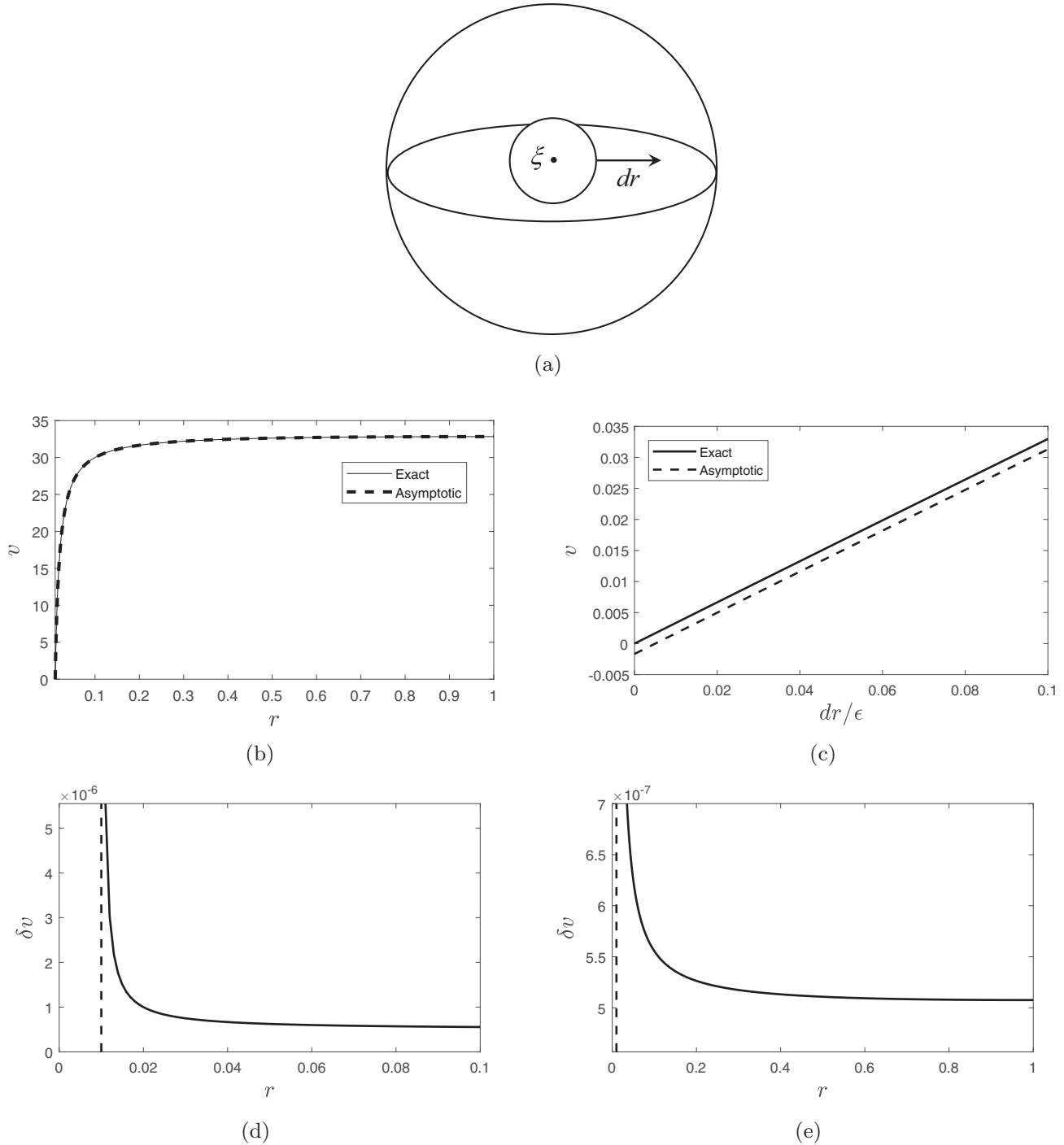


FIG. 4. (a) A single trap of radius ϵ , centered at the origin. (b) Asymptotic vs exact MFPT for a trap of radius $\epsilon = 10^{-2}$. (c) Asymptotic vs exact MFPT in the region near a trap of radius $\epsilon = 10^{-1}$, with the distance from the surface of the trap represented relative to the size of the trap, $dr = r - \epsilon$. (d) The error in the asymptotic MFPT, relative to the exact MFPT, as a function of position in the domain, for a trap of radius $\epsilon = 10^{-2}$. The surface of the trap is indicated by a dotted line. (e) Same as panel (d), rescaled to show the behavior of δv away from the trap.

The comparison results between the asymptotic MFPT formulas (2.2) and the exact solution (2.1) (single central trap) or numerical solutions indicate that the asymptotic solutions provide a close approximation of the mean first passage time MFPT, remaining valid even when the assumptions of traps being “small,” “well separated,” and “far from the boundary” are violated; that is, the applicability of the asymptotic MFPT formulas (2.2) extends well beyond their derivation

assumption. In particular, the comparisons may be summarized as follows:

- (1) For a single central trap of radius $\epsilon = 10^{-2}$, the relative error between asymptotic and exact MFPT formulas (2.2a), (2.1a) is $\delta v(x) \lesssim 10^{-6}$ for the points x located at distances $dr \geq \epsilon$ from the trap surface, i.e., $|x| \geq 2\epsilon$.
- (2) The approximation of the average MFPT provided by the asymptotic formula (2.2b) for a single centered trap stays

within 1% relative error from the exact solution (2.1b) for trap sizes as large as $\epsilon \lesssim 0.2$, i.e., 20% of the radius of the domain.

(3) For two traps of radius $\epsilon = 10^{-2}$ located away from the domain center and the boundary, the relative difference between the asymptotic and numerical MFPT is within 1% for distances $d \gtrsim \epsilon$ between trap surfaces.

(4) For a single small trap approaching the reflective domain boundary, the discrepancy between the asymptotic AMFPT formula (2.2b) and the numerical solution grows the same way as when two traps approach each other. For a small trap of radius $\epsilon = 10^{-2}$, the relative error stays within 1% when the trap is further than about $\epsilon/2$ from the boundary.

A. The asymptotic MFPT error as a function of the position in the domain

To determine how the error δv depends on the position in the domain, the asymptotic MFPT $v_A(x)$ (2.2a) can be compared to the exact solution $v_e(x)$ for a single spherical trap of radius ϵ centered at the origin of the unit sphere. One has $c = 1$, and the asymptotic MFPT formulas (2.2) can be directly evaluated to give

$$v_{A_1} = \frac{1}{6D} \left[\frac{2}{\epsilon} - \frac{r^3 + 2}{r} \right], \quad (3.2a)$$

$$\bar{v}_{A_1} = \frac{1}{6D} \left[\frac{2}{\epsilon} - \frac{18}{5} \right]; \quad (3.2b)$$

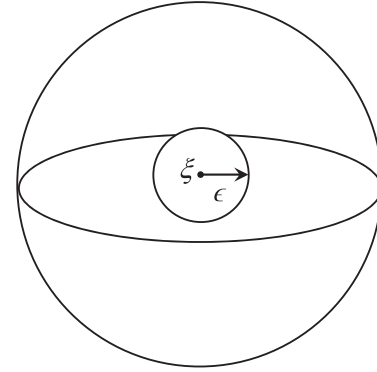
whereas the exact MFPT and AMFPT are given by (2.1). Due to the spherical symmetry of this configuration, the asymptotic MFPT and the error term δv may depend only on the radial distance r from the origin.

By comparison of (III.2) to (2.1), it can be shown that the asymptotic approximation is exact only when $\epsilon = 0$. It is also evident that the boundary condition $v = 0$ on the surface of the trap will not be satisfied by (3.2a) unless $\epsilon = 0$. In addition, from (3.2b) we observe for $\epsilon \geq 5/9$ that the approximate AMFPT becomes negative, which is a consequence of the singular term of the Green's function, and the related validity of the asymptotic MFPT solution only "far" from the trap.

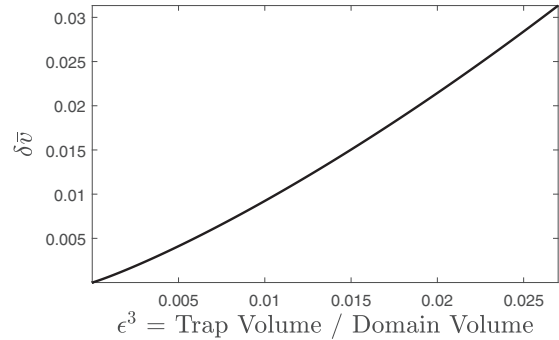
Furthermore, we observe that for this single trap, the absolute error of the approximation is in fact constant, given by

$$\Delta v_1 = \Delta \bar{v}_1 = |v_{A_1} - v_e| = |\bar{v}_{A_1} - \bar{v}_e| = \frac{\epsilon^3}{6D}. \quad (3.3)$$

The configuration is shown in Fig. 4(a). For a trap of radius $\epsilon = 10^{-2}$, Fig. 4(b) shows that the asymptotic MFPT is close to the exact MFPT throughout the domain, and Fig. 4(c) illustrates the constant error $\Delta v_1 = O(\epsilon^3)$ throughout the spherical domain for $\epsilon = 10^{-1}$, with the distance from the trap being represented relative to the size of the trap: dr/ϵ , $dr = r - \epsilon$. Figures 4(d) and 4(e) again use $\epsilon = 10^{-2}$, and show the relative error (3.1a) of the asymptotic approximation as a function of r . The error grows quickly when one approaches the trap boundary and is bounded away from the trap. In particular, for the points x as close to the trap as $dr = \epsilon$, the relative error is rather small, $\delta v \lesssim 10^{-6}$.



(a)



(b)

FIG. 5. (a) A single trap of radius ϵ centered at the origin. (b) The relative error $\delta \bar{v}$ (3.1b) between the asymptotic AMFPT (2.2b) and the exact solution (2.1), as a function of the trap volume.

B. Effects of trap size

To determine the accuracy of the asymptotic approximation with respect to the size of the traps, we compute the error $\delta \bar{v}$ (3.1b), relative to the exact solution \bar{v}_e , for a single spherical trap of radius ϵ centered at the origin of the unit sphere, as a function of the trap size $\epsilon \in [0, 0.1]$. Figure 5 depicts the relationship between $\delta \bar{v}$ and the relative trap volume ϵ^3 . It is observed that the error $\delta \bar{v}$ grows almost linearly with the trap volume, at a rate of approximately 0.69% per unit trap volume ratio. Based on the comparisons, one may conclude that the approximation of the average MFPT provided by the explicitly known terms of the formula (2.2b) is valid within 1% precision for trap radii $\epsilon \lesssim 0.2$, i.e., for traps of linear dimension about 20% of that of the domain.

C. Effects of trap separation

In order to analyze the quality of approximation provided by the asymptotic solution (2.2a) of the narrow capture problem (1.1), we analyze the behavior of the relative error $\delta \bar{v}$ as a function of the distance between two identical traps. We pick "small" identical traps of radius $\epsilon = 10^{-2}$ fixed at the distance $r_1 = r_2 = 10\epsilon$ from the sphere center, located at the equatorial plane (spherical polar angles $\theta_1 = \theta_2 = \frac{\pi}{2}$). Let the azimuthal angle $\phi_1 = 0$. The angle between the two traps is given by the azimuthal angle $\phi = \phi_2$ of the second trap. We let the angle

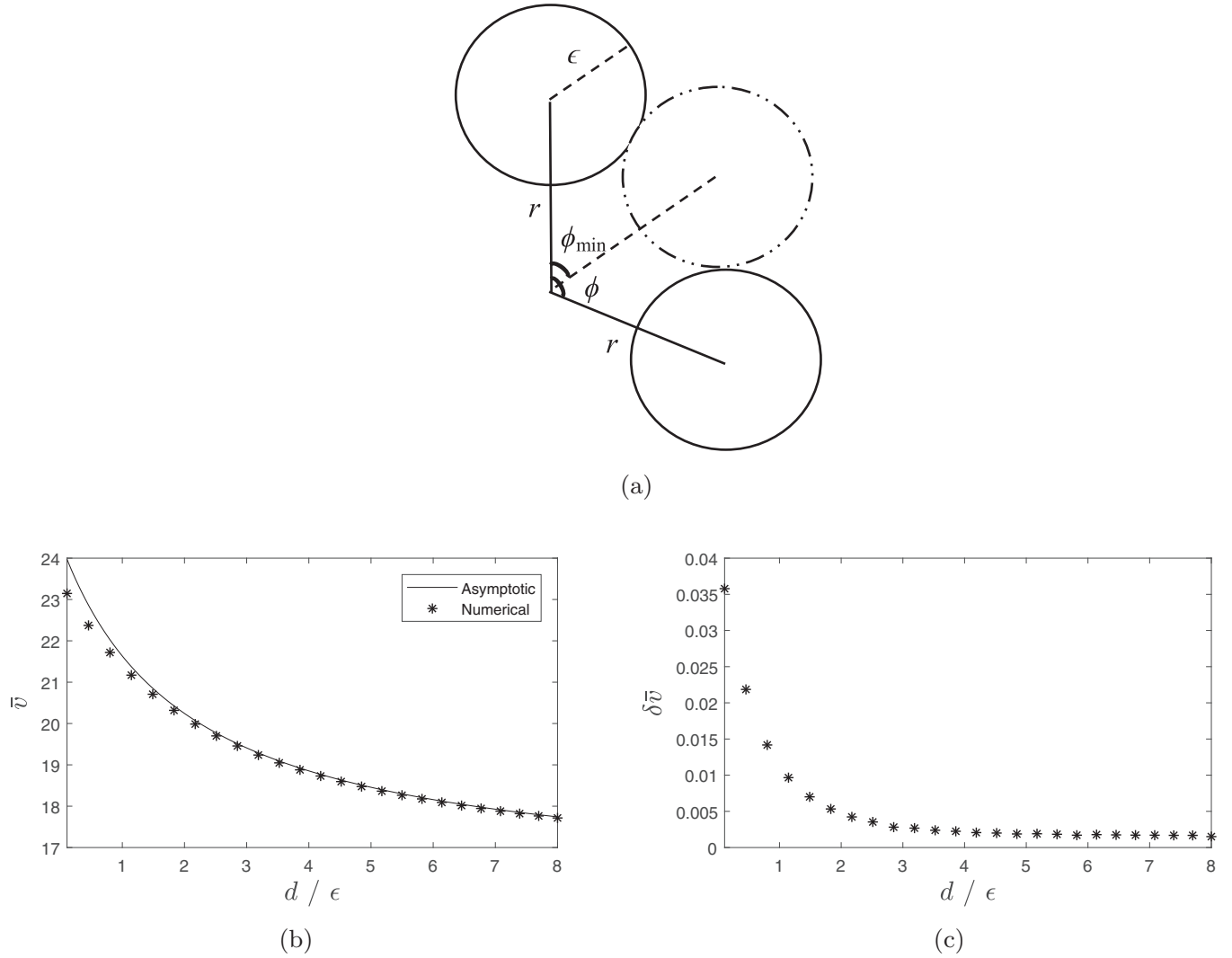


FIG. 6. (a) The two-trap configuration used to test the accuracy of the asymptotic approximation with respect to the trap separation distance. (b) A comparison of the asymptotic and numerical AMFPT as a function of the trap separation d/ϵ . (c) The relative difference of the asymptotic and numerical AMFPT as a function of d/ϵ .

ϕ_2 be varied between $1.05 \times \phi_{\min} \leq \phi_2 \leq \pi$, where ϕ_{\min} is the angle at which the traps come into contact [Fig. 6(a)]. The shortest distance between the trap boundaries is given by

$$d = r\sqrt{2(1 - \cos \phi)} - 2\epsilon. \quad (3.4)$$

Figure 6(b) shows the dependence of the asymptotic AMFPT \bar{v}_A and the numerical AMFPT \bar{v}_N on the trap separation distance measured in units of trap size ϵ , while Fig. 6(c) contains the corresponding plot of the relative AMFPT difference $\delta \bar{v}$ (3.1b).

From the comparison it is observed that the relative difference between the asymptotic and numerical MFPT is already within 1% for $d \gtrsim \epsilon$; that is, the asymptotic formula (2.2b) provides a decent approximation of the average MFPT even for rather closely located traps.

Since in the current setup the traps are always located at the same distance from the domain boundary, the boundary effects on the approximation error are essentially absent (such effects are separately studied in the following subsection). We

also note that the contribution of the numerical error in Fig. 6 is not dominant; indeed, for a single centered spherical trap of radius $\epsilon = 10^{-2}$, where the exact solution is known, the relative numerical error of a similar finite-element computation does not exceed the order of 10^{-3} .

D. Effects of the boundary proximity

Finally, we examine how the proximity of a trap to the reflective domain boundary influences the accuracy of the approximate asymptotic AMFPT (2.2b). Indeed, in the asymptotic MFPT formulas (2.3), in particular, in the trap interaction energy (2.4), the first two terms of the Green's function (2.3a) involve both the trap position and the symmetric point with respect to the spherical domain boundary. This corresponds to every trap “interacting” with its “reflection”—a virtual trap located at a point symmetric with respect to the unit sphere—in a similar way it would interact with another trap. This suggests that as the trap approaches the boundary of the domain, the error of approximation provided by the known

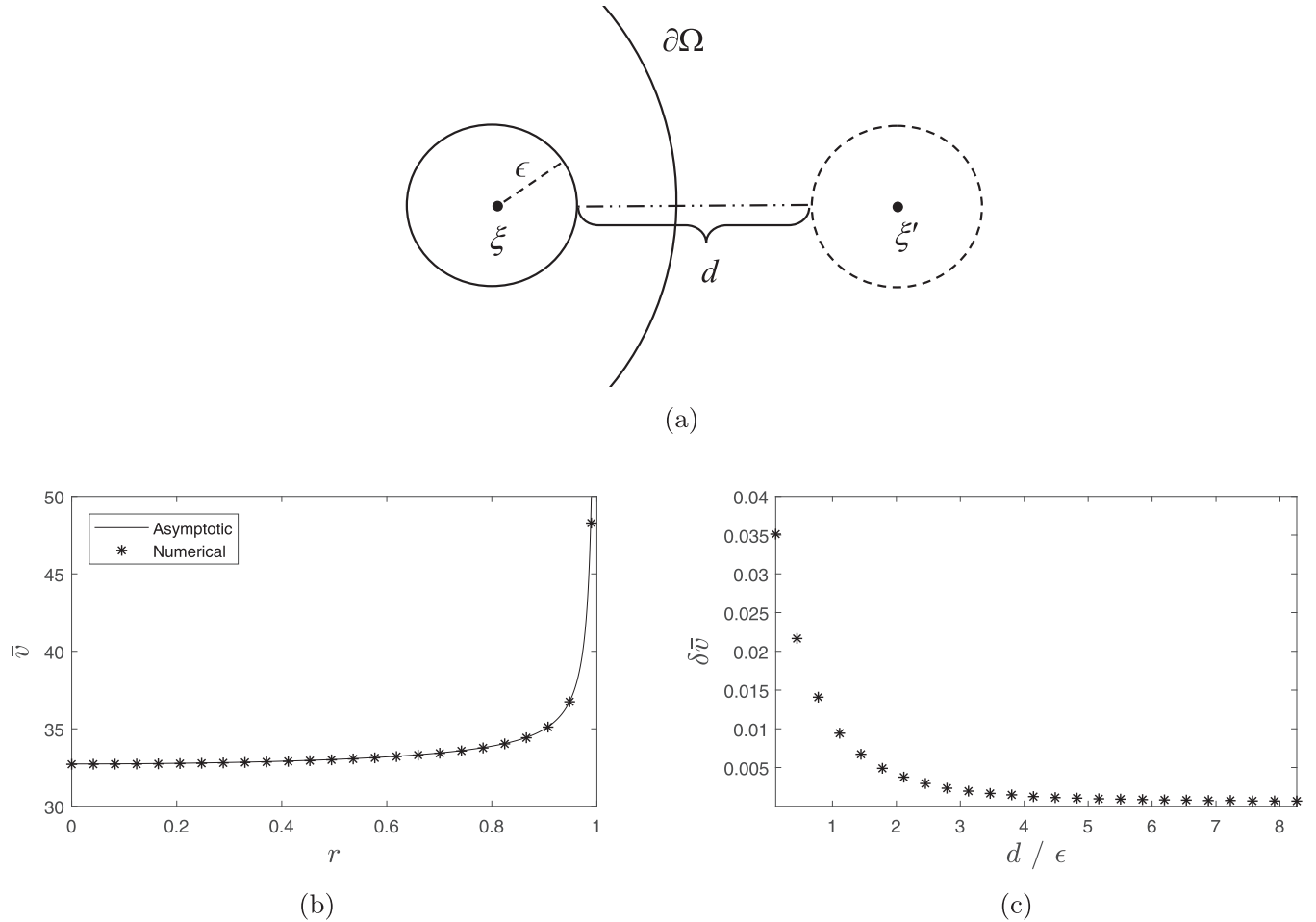


FIG. 7. (a) A trap and its image. Here d is the separation between the two boundaries. (b) A side-by-side comparison of the asymptotic AMFPT (2.2b) and the numerical AMFPT. (c) The difference between the asymptotic and numerical AMFPT, relative to the numerical approximation (3.1b), as a function of the relative distance d/ϵ between the trap and its image. The absolute trap-to-image distance d is given by (3.5).

leading terms of the asymptotic AMFPT (2.2b) may increase, as if the distance between a trap pair were decreasing.

In order to study the trap-reflection interaction effects, the relationship between $\delta\bar{v}$ and the position of a trap (ξ) within the domain of the unit sphere was examined by varying ξ radially from the origin to $1 - 1.05\epsilon$, to keep the trap and its image from contact, for a single trap of a fixed radius $\epsilon = 10^{-2}$ [Fig. 7(a)].

As the trap approaches the boundary, the discrepancy $\delta\bar{v}$ between the asymptotic and numerical solutions \bar{v}_A , \bar{v}_N increases and can be easily distinguished from the numerical error present in \bar{v}_N . Figures 7(b) and 7(c) show \bar{v}_A , \bar{v}_N and their relative difference $\delta\bar{v}$ as functions of the distance between the trap and its image, defined as

$$d = x^{-1} - x - 2\epsilon. \quad (3.5)$$

It is observed that the relative difference $\delta\bar{v}$ between \bar{v}_A and \bar{v}_N is below 1% already for $d \gtrsim \epsilon$, i.e., when the trap “almost touches” the domain boundary. In particular, we note that the error plots in Figs. 6(c) and 7(c) are virtually indistinguishable, hence the trap-trap and trap-reflection interactions indeed have a similar effect on MFPT, at least at small separation distances.

IV. OPTIMAL CONFIGURATIONS OF MULTIPLE TRAPS

A. The optimization approach

For a given set of N traps that may move in a particular physical domain, higher values of the average mean first passage time (1.2) correspond to the situations when traps are small, or clustered together, located in domain “corners,” or are otherwise “hard to find” for an average Brownian particle that begins its journey from some point x_0 in the domain. A question of practical interest is:

What trap arrangement minimizes the AMFPT?

This is the simplest of the global optimization questions, since it involves only a single scalar value \bar{v} to be optimized as a function of $3N$ trap locations. The “simplest” problem setup is finding such optimal arrangements when N traps are identical and a domain has a simpler geometry, such as a unit sphere. Harder practically relevant optimization questions would include optimizations of nonscalar quantities related to $v(x)$, nonequal traps, extensions to moving traps and domains changing in time, etc.

Yet even in the simplest setup, when N small identical traps are placed to minimize the AMFPT (1.2) in a domain as simple as the unit sphere, neither the analytical solution of the

optimization problem nor even a general closed-form exact solution $v(x)$ of the MFPT problem (1.1), are known. The AMFPT optimization using, for example, a numerical solution of the MFPT problem (1.1) would involve multiple sampling the AMFPT \bar{v} in its $3N$ -dimensional domain, resulting in a high number of separate time-consuming numerical solutions of the BVP (1.1). The numerical problem becomes even more difficult when traps are small, since those would require extensive mesh refinement near the traps.

By contrast, the asymptotic solution \bar{v}_A (2.2b) is directly suitable for global optimization with respect to locations of N (identical or nonidentical) traps, since it involves an explicit trap interaction term (2.4) given in terms of a known spherical Neumann Green's function (2.3). In Sec. III we have verified that the asymptotic MFPT formulas are suitable in terms of approximation precision. We now proceed to use these approximations to compute the optimal trap arrangements in a unit sphere.

To answer the basic question, we seek optimal spherical arrangements of N equal-strength traps ($c_j \equiv 1$) minimizing the AMFPT \bar{v}_A (2.2b), or equivalently, the quantity

$$\mathcal{H}_{\text{ball}} = 4\pi p_c + \frac{14}{5}N^2, \quad (4.1)$$

with respect to trap positions.

In Ref. [24] numerical optimization of $\mathcal{H}_{\text{ball}}$ was carried out for $2 \leq N \leq 20$ traps in a much simpler, constrained setup: it was assumed that all traps lie on a single nested sphere of radius $0 < r < 1$, with perhaps one trap lying at the origin; free implementations of ECAM and DSO numerical optimization software algorithms were used. In the current study, we perform a full three-dimensional optimization of $N \leq 100$ traps.

Inside the unit sphere, the location of each of the traps ξ_j is given by its spherical coordinates (r_j, θ_j, ϕ_j) . In order to eliminate the continuous rotational symmetry of the spherical domain, the trap ξ_1 may be fixed at the z axis by taking $\theta_1 = \phi_1 = 0$, and the trap ξ_2 may be forced to lie in the x - z plane by taking the azimuthal coordinate $\phi_2 = 0$. [We note that the reflection symmetries will indeed remain.] Consequently, for N traps, the global optimization problem involves minimizing $\mathcal{H}_{\text{ball}}$ as a function of $3N - 3$ parameters within the bounds

$$\begin{aligned} 0 \leq r_j < 1, \quad j = 1, \dots, N; \quad 0 < \theta_j \leq \pi, \quad j = 2, \dots, N; \\ 0 < \phi_j \leq 2\pi, \quad j = 3, \dots, N. \end{aligned}$$

Due to the high dimensionality of the problem, the number of local minima grows quickly with N . These local minima may lie very near the global minima, or one another. Nevertheless, the putative optima reported below give insights into the nature of the optimal trap configurations, if not the exact coordinates of each trap.

Trap configurations which minimized $\mathcal{H}_{\text{ball}}$ were sought using a Matlab interface for a Lipschitz-continuous global optimizer (LGO) [31]. LGO software is one of the most efficient global optimizers. It seeks the putative solution of constrained global optimization problems using a combination of global and local search algorithms. The input includes the starting, or “nominal,” configuration, with which LGO begins its search. Experimentation showed that for the optimization procedure

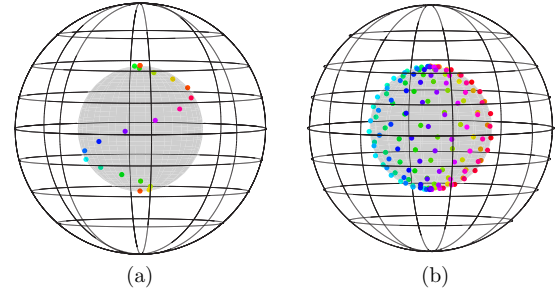


FIG. 8. Sample starting configurations for $N = 20$ (a) and $N = 150$ (b), with traps colored according to the azimuthal angle ϕ . The traps are located on spirals about the surface of a sphere of $r = 0.5$.

described below, the results do not depend on the starting configuration, as long as the latter are sufficiently spaced out; the global sampling is performed by LGO throughout the function domain. From the results of Ref. [24] and references therein, as well as the results of two-dimensional global optimization in a disk [25], it can be conjectured that optimal trap arrangements within a spherical domain may be close to those which distribute the traps over surfaces of some smaller spheres nested within the given one. We will refer to those as “shells” and use the notation

$$r_k^\circ = \frac{1}{N_k^\circ} \sum_{j=1}^{N_k^\circ} r_j^\circ. \quad (4.2)$$

In (4.2), r_k° is the radius of the k th shell, N_k° is the number of traps on the k th shell, and r_j° is the radial coordinate of the j th trap on the k th shell.

It is well known that “homogeneous” arrangements of points on a sphere may be obtained using spiral designs. The starting configurations were chosen so that the unconstrained traps were distributed across spirals on a shell of radius 0.5, with the angular coordinates depending on N . The coordinates of the traps on the shell are given by

$$r_j = 0.5, \quad \theta_j = \frac{2\pi j}{N-2}, \quad \phi_j = \frac{100N\pi j}{N-3} \pmod{2\pi}, \quad (4.3)$$

shown in Fig. 8.

The optimization procedure. In order to seek the optimal arrangement of N traps, the optimization was carried out in two stages, referred to as the *search stage* and *refinement stage*. The important parameters of the LGO algorithm employed in the optimization include the global function evaluations (GFE), the local function evaluations (LFE), and the number of iterations without improvement (IWI). The search stage took a large number of GFE ($\sim 10^8$) and a small number of LFE and IWI ($\sim 10^4$). These parameters were chosen to perform a superficial, but broad, investigation of the parameter space. Relative to the search stage, the refinement stage took a moderate number of GFE ($\sim 10^6$), a larger number of LFE ($\sim 10^6$), and a similar number of IWI ($\sim 10^4$). These parameters were chosen to perform a more thorough search in the vicinity of promising configurations found during the search stage. The optimization routine carries out iterative sweeps of the parameter space, with the nominal configurations of the first search sweep being the spirals defined in (4.3), and the

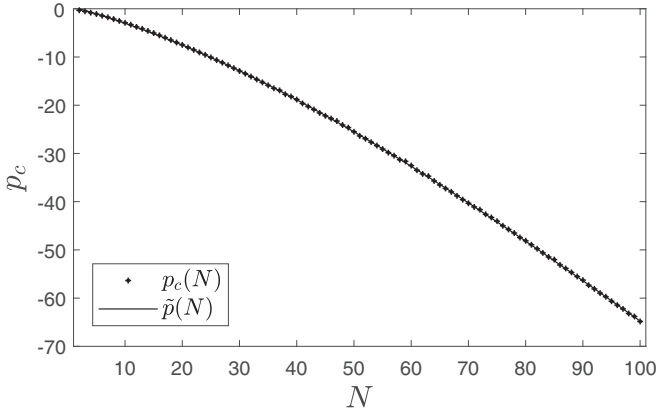


FIG. 9. The interaction energy p_c (2.4) and the cubic polynomial interpolant $\tilde{p}(N)$ (4.4) for the putative optimal configuration of N equal traps ($c_j = 1$) minimizing the AMFPT for the unit sphere.

best results from the previous sweep being taken as the nominal for the next sweep. Search sweeps were performed until a trap configuration giving $p_c \leq 0$ was first discovered, as this was found to be a characteristic of the optimal configuration determined earlier (see Fig. 9). After that, refinement sweeps were performed until the changes in p_c between each sweep became small (typically $\sim 10^{-7}$).

In the following subsections, the above-described global optimization procedure is used to compute N trap arrangements, $2 \leq N \leq 100$, corresponding to putative minima of the asymptotic AMFPT \bar{v}_A (2.2b) or, equivalently, the trap interaction energy p_c given by (2.4). It is shown that $p_c(N)$ is a decreasing function, and a cubic interpolation polynomial is computed. The computed putative global minima for $N \leq 20$ are shown to yield lower energy values than the configurations obtained by constrained optimization in Ref. [24]. For $N \leq 23$, traps in the optimal configurations are found to lie around (though not exactly on) a single spherical shell within the unit sphere domain. For $N \geq 24$, traps may be located in a close vicinity of two or three nested spherical shells.

B. Putative optimal configurations for $N \leq 100$

Though the search algorithm implementation minimizes $\mathcal{H}_{\text{ball}}$ (4.1), it is more meaningful to discuss the configurations in terms of the values of trap interaction energy p_c given by (2.4). From a plot of p_c for $2 \leq N \leq 100$, shown in Fig. 9, it can be seen that the interaction energy for an optimal configuration is monotone decreasing. In particular, based on the data presented below, the Matlab polyfit routine yields the cubic interpolation curve described by

$$\tilde{p}(N) \sim 1.47246 \times 10^{-5} N^3 - 4.82389 \times 10^{-3} N^2 - 3.18915 N + 6.53625 \times 10^{-1}. \quad (4.4)$$

This relationship was used to estimate the globally optimal values of p_c for consequent computations and to more efficiently guide the optimization routine as N grew large.

TABLE II. A comparison of putative optimal interaction energy values p_c (2.4) for N equal traps ($c_j = 1$), $5 \leq N \leq 23$, obtained using the general three-dimensional unconstrained optimizations (column 1) vs two constrained optimizations of Ref. [24]: all traps on a spherical shell (column 2) and one centered trap with $N - 1$ traps on a spherical shell (column 3). The lowest value [the putative global energy minimum of the interaction energy values p_c (2.4)] is shown in boldface.

| N | No constraint | One shell | Trap at origin |
|----|-------------------|---------------------|--------------------------------------|
| | r_1, \dots, r_N | $r_1 = \dots = r_N$ | $r_2 = \dots = r_N$ ($r_1 = 0$) |
| 5 | -1.09668 | -1.09667 | -0.94042 |
| 6 | -1.44441 | -1.44441 | -1.25076 |
| 7 | -1.76390 | -1.76522 | -1.62993 |
| 8 | -2.13677 | -2.13455 | -1.98057 |
| 9 | -2.52013 | -2.52011 | -2.36166 |
| 10 | -2.91473 | -2.91471 | -2.79922 |
| 11 | -3.30392 | -3.30388 | -3.22597 |
| 12 | -3.76236 | -3.76236 | -3.64697 |
| 13 | -4.15781 | -4.15792 | -4.13912 |
| 14 | -4.59881 | -4.59872 | -4.56650 |
| 15 | -5.04074 | -5.04122 | -5.04014 |
| 16 | -5.51557 | -5.49573 | -5.51546 |
| 17 | -6.00303 | -5.95685 | -6.00278 |
| 18 | -6.49702 | -6.42519 | -6.49697 |
| 19 | -6.99849 | -6.87892 | -6.99845 |
| 20 | -7.48530 | -7.37047 | -7.48503 |
| 21 | -8.00992 | -7.84980 | -8.00968 |
| 22 | -8.52223 | -8.33926 | -8.52215 |
| 23 | -9.04471 | -8.80148 | -9.04517 |

C. Radial distribution of traps in optimal configurations ($N \leq 23$)

First we use the above-described procedure to perform a full three-dimensional search of putative globally optimal configurations of N identical traps minimizing the AMFPT (1.2) for lower values of N , in order to compare the results with those obtained in a constrained optimization in Ref. [24], where all traps, except for possibly a single central one, were constrained to a surface of a single spherical shell of radius $0 < r < 1$. In Ref. [24] it was shown that between these two constrained scenarios, for $N < 16$, configurations with no central trap yielded lower values of \bar{v} , whereas for $16 \leq N \leq 20$ traps, configurations with one trap centered at the origin were preferred.

In Table II we show that for $5 \leq N \leq 23$, in 13 out of 19 cases, the full three-dimensional unconstrained optimization yields lower minimum values of p_c (AMFPT) than both constrained situations. (The column “one shell” refers to the case when all traps are fixed on a single shell: $r_1 = \dots = r_N$, giving $2N - 2$ optimization parameters; the column “trap at origin” corresponds to all traps on a single shell with one trap at the origin: $r_1 = 0, r_2 = \dots = r_N$ with $2N - 4$ optimization parameters.)

The results described above do not mean that the distribution of traps over the surface of a sphere is the optimal arrangement in six of the 19 cases; rather, these values were obtained by allowing the search algorithm described in Sec. IV A to run the same number of sweeps on each case

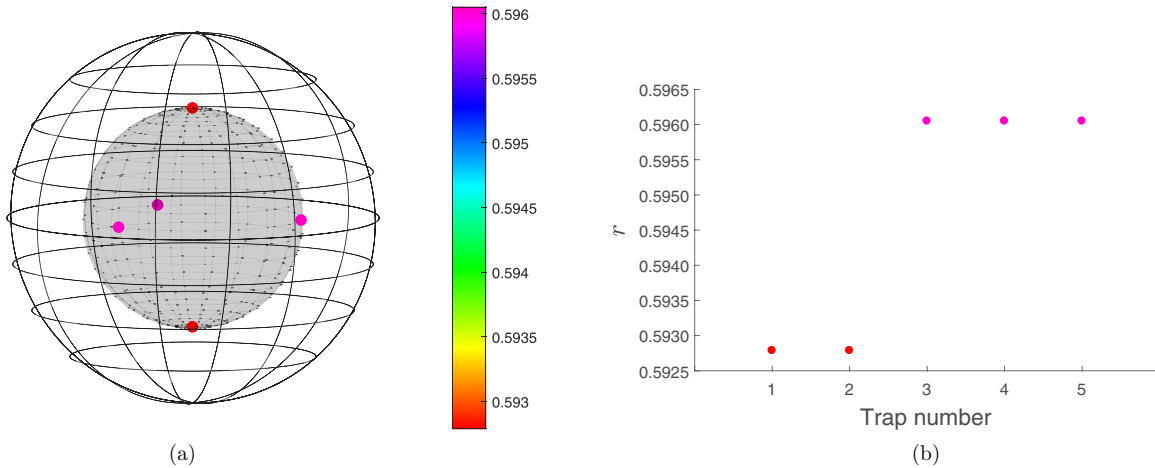


FIG. 10. (a) The putative optimal trap configuration and (b) radial distribution of traps for $N = 5$, showing two discrete radial distances of traps located closely to a single “shell” [see (4.2)]. Three traps are found at the equator at a common distance, while two traps are found along the z axis at a common distance.

of constraint using the best result found between all cases as the nominal configuration for each case in the next sweep. Comparing the six questionable values of N found in Table II to the final putative optimums given in Table III, it can be seen that in all cases the unconstrained search gives the lowest minimum value of p_c .

The search routine was tested to see if it would be advantageous to first search for a constrained optimum, then use the configuration obtained there as a nominal configuration for an unconstrained search. The idea behind it is that if the constrained and unconstrained optimal configurations were near enough to each other, the majority of the search could be carried out using the lower-dimensional problem, and then that neighborhood of the parameter space could be searched using the higher-dimensional unconstrained problem. It was found that this search routine was able to converge to the neighborhood of the optimum more quickly, but the overall search time did not decrease appreciably.

Interestingly, it appears that in most cases, the optimal configuration is one which the traps are distributed discretely across a narrow range of r , so indeed, in most numerical

globally optimal configurations, traps are located close to being on a single or multiple, sometimes extremely closely located, spherical shells. This is illustrated for $N = 5$, $N = 8$, and $N = 19$ in Figs. 10–12.

We note that the range of r the traps are found within does not clearly reflect the variation in p_c between the constrained optimal configuration and the unconstrained optimal configuration. Compared to the p_c associated with a constrained optimal configuration, a small ($\sim 10^{-7}$) range of varying radial trap positions r may give a significant difference in p_c for some N ($\sim 10^{-2} \dots 10^{-4}$), while a larger ($\sim 10^{-3}$) range of r can result in a small difference in p_c for other N ($\sim 10^{-4} \dots 10^{-7}$). It should be noted that the relative differences in p_c values between constrained and unconstrained configurations ($\sim 10^{-3} \dots 10^{-4}$) are relatively small, though the similarities between the unconstrained trap configurations imply that the optimal configuration is often likely to be one which distributes the traps over several values of r . This relationship between p_c and r implies that for some N the optimal configuration is more similar to a spherical shell than other N .

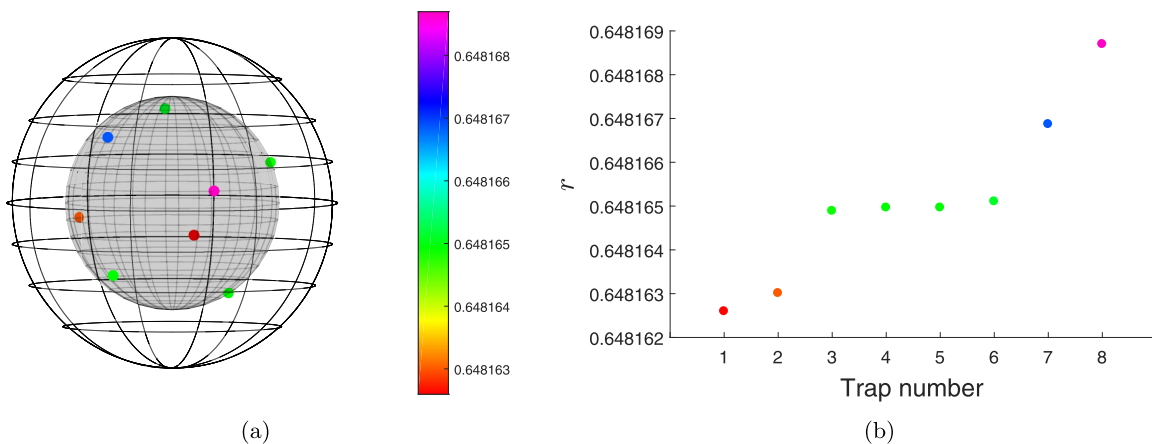


FIG. 11. (a) The putative optimal trap configuration and (b) radial distribution of traps for $N = 8$, showing five discrete radial distances of traps located closely about a single “shell” [see (4.2)].

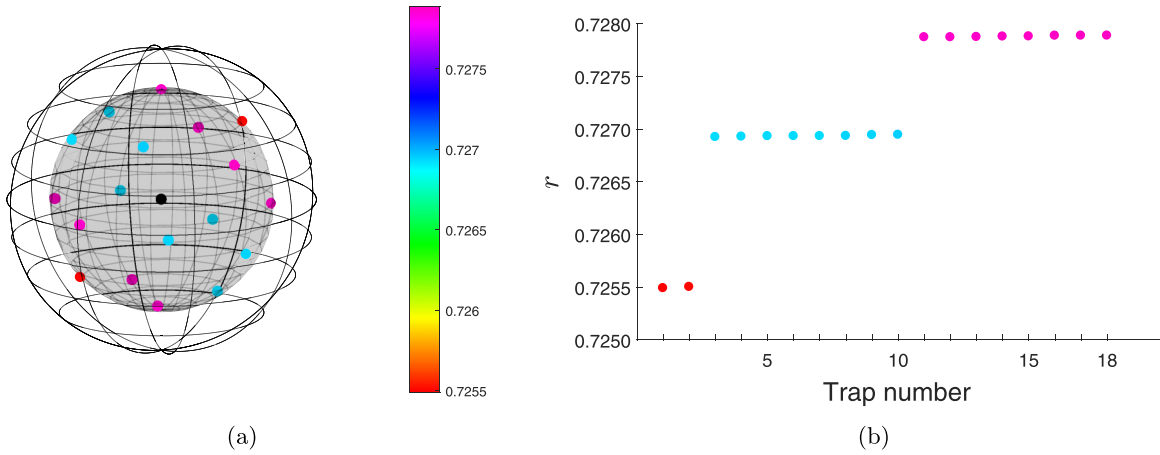


FIG. 12. (a) The putative optimal trap configuration and (b) radial distribution of traps excluding the origin for $N = 19$, showing three characteristic spherical shell radii of traps located closely about a single “shell”; see (4.2).

D. Radial distribution of traps in optimal configurations
($N \geq 24$)

The first trap configuration which significantly differs from those previously studied in Ref. [24] for $N \leq 20$ is $N = 24$. Here all but two of the traps are distributed about a shell of $r = 0.763$, while the others are found at the poles of a shell with $r = 0.226$. From a plot of the radial coordinates of each of the traps for $N = 24$, shown in Fig. 13, it can be seen that the traps located about the outer shell do not lie exactly on the shell. Similar to the radially unconstrained configurations discussed for $N \leq 23$, the traps on the outer shell are distributed over a small range of discrete values of r . $N = 25$ is the largest value of N for which a single shell is observed, with 24 of the traps located on a shell $r = 0.736$ and one shell at the origin. For all $N > 25$ which were examined, the optimal configuration was one which distributed the traps over several shells, with or without a trap at the origin.

In order to concisely describe the optimal trap configurations, the following notation will be used. The presence of trap at the origin will be indicated in the subscript, where “•” denotes a trap at the origin, and “o” denotes otherwise. The

number of shells in a configuration will be indicated in normal type. The number of traps on each shell will be indicated by a list in superscript, in order of smallest to largest radius of shells. For example, the configuration code notation for $N = 24$ and $N = 25$ would be the following:

$$N_{24} = \text{o}2^{[2,22]}, \quad N_{25} = \bullet 1^{[24]}. \quad (4.5)$$

A plot of the how traps are distributed across shells for each $2 \leq N \leq 100$ can be found in Fig. 14, and a plot of the radius of each shell, defined as (4.2), can be found in Fig. 15. From these plots it can be seen that, in general, the size of the shell is proportional to the number of traps associated with it. For some N , such as 59, this trend does not hold. In such cases a single trap can be found between two shells.

Cursory computations of optimal configurations for $N = 200, 250, 300, 350, \dots, 500$ have also been performed but are not presented here. The form of optimal configurations of $N > 100$ traps is not yet well understood, making it difficult to say with confidence that these configurations are the optimal ones. To speculate on the form these configurations may take, for $N > 100$ we expect that the nested shell structure

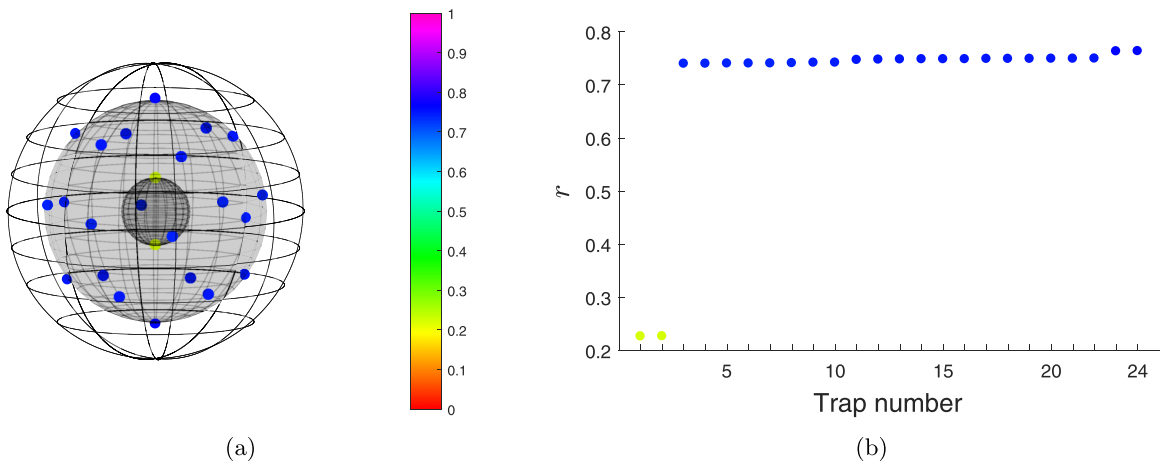


FIG. 13. (a) The putative optimal trap configuration and (b) radial distribution of traps excluding the origin for $N = 24$, the traps distributed near two clearly different nested spherical “shells”; see (4.2).

TABLE III. Interaction energy and radial distribution of traps for putative optimal trap configurations for $2 \leq N \leq 100$. For each optimal trap configuration, the traps are located in one, two, or three nested spherical “shells” [see (4.2)]; the configuration codes (4.5) contain the numbers of traps in each shell. The radial trap distributions are illustrated in Figs. 14 and 15.

| N | p_c | Code | N | p_c | Code | N | p_c | Code |
|-----|-----------|----------------------|-----|-----------|--------------------------|-----|-----------|-------------------------|
| 2 | -0.31224 | ◦1 ^[2] | 35 | -15.88018 | ◦2 ^[4,31] | 68 | -38.79978 | ◦2 ^[14,53] |
| 3 | -0.53279 | ◦1 ^[3] | 36 | -16.48464 | ◦2 ^[5,31] | 69 | -39.58469 | ◦2 ^[15,53] |
| 4 | -0.81459 | ◦1 ^[4] | 37 | -16.92749 | ◦2 ^[4,32] | 70 | -40.33126 | ◦2 ^[14,55] |
| 5 | -1.09668 | ◦1 ^[5] | 38 | -17.72523 | ◦2 ^[5,33] | 71 | -41.09708 | ◦2 ^[15,55] |
| 6 | -1.44441 | ◦1 ^[6] | 39 | -18.19441 | ◦2 ^[5,33] | 72 | -41.65766 | ◦3 ^[1,14,56] |
| 7 | -1.76531 | ◦1 ^[7] | 40 | -18.83246 | ◦2 ^[5,34] | 73 | -42.61921 | ◦2 ^[16,56] |
| 8 | -2.13677 | ◦1 ^[8] | 41 | -19.62695 | ◦2 ^[6,35] | 74 | -43.28359 | ◦3 ^[2,17,55] |
| 9 | -2.52013 | ◦1 ^[9] | 42 | -20.26309 | ◦2 ^[7,35] | 75 | -44.04266 | ◦3 ^[2,17,56] |
| 10 | -2.91474 | ◦1 ^[10] | 43 | -20.89590 | ◦2 ^[7,36] | 76 | -45.00034 | ◦2 ^[18,57] |
| 11 | -3.30396 | ◦1 ^[11] | 44 | -21.59580 | ◦2 ^[7,37] | 77 | -45.75273 | ◦2 ^[17,59] |
| 12 | -3.76236 | ◦1 ^[12] | 45 | -22.20394 | ◦2 ^[8,37] | 78 | -46.50311 | ◦2 ^[17,60] |
| 13 | -4.15808 | ◦1 ^[13] | 46 | -22.77657 | ◦2 ^[7,38] | 79 | -47.43354 | ◦2 ^[17,61] |
| 14 | -4.59883 | ◦1 ^[14] | 47 | -23.28838 | ◦3 ^[2,7,38] | 80 | -48.11157 | ◦3 ^[2,18,60] |
| 15 | -5.04138 | ◦1 ^[15] | 48 | -24.11670 | ◦2 ^[9,38] | 81 | -48.93729 | ◦2 ^[20,60] |
| 16 | -5.51557 | ◦1 ^[15] | 49 | -24.85055 | ◦2 ^[8,40] | 82 | -49.76916 | ◦3 ^[2,19,61] |
| 17 | -6.00303 | ◦1 ^[16] | 50 | -25.51602 | ◦2 ^[10,39] | 83 | -50.62332 | ◦2 ^[18,64] |
| 18 | -6.49702 | ◦1 ^[17] | 51 | -26.36141 | ◦2 ^[10,41] | 84 | -51.46399 | ◦2 ^[21,62] |
| 19 | -6.99849 | ◦1 ^[18] | 52 | -26.94522 | ◦2 ^[9,42] | 85 | -52.01166 | ◦3 ^[2,20,62] |
| 20 | -7.48530 | ◦1 ^[19] | 53 | -27.67077 | ◦2 ^[10,42] | 86 | -53.12100 | ◦2 ^[21,64] |
| 21 | -8.00992 | ◦1 ^[20] | 54 | -28.37220 | ◦2 ^[10,43] | 87 | -53.85227 | ◦2 ^[22,64] |
| 22 | -8.52231 | ◦1 ^[21] | 55 | -29.09366 | ◦2 ^[10,44] | 88 | -54.66680 | ◦3 ^[2,20,66] |
| 23 | -9.04517 | ◦1 ^[22] | 56 | -29.82679 | ◦2 ^[10,45] | 89 | -55.52195 | ◦3 ^[2,21,66] |
| 24 | -9.55173 | ◦2 ^[2,22] | 57 | -30.46590 | ◦2 ^[13,43] | 90 | -56.26874 | ◦3 ^[1,23,65] |
| 25 | -10.09123 | ◦1 ^[24] | 58 | -31.29196 | ◦2 ^[12,45] | 91 | -57.32729 | ◦3 ^[2,21,68] |
| 26 | -10.65106 | ◦2 ^[2,24] | 59 | -31.64227 | ◦4 ^[1,8,1,48] | 92 | -58.08717 | ◦3 ^[1,22,68] |
| 27 | -11.18152 | ◦2 ^[2,25] | 60 | -32.51241 | ◦3 ^[2,12,46] | 93 | -58.96340 | ◦3 ^[3,24,66] |
| 28 | -11.73199 | ◦2 ^[2,26] | 61 | -33.47995 | ◦2 ^[12,48] | 94 | -59.71180 | ◦3 ^[1,24,68] |
| 29 | -12.31676 | ◦2 ^[2,27] | 62 | -34.24925 | ◦2 ^[12,49] | 95 | -60.64756 | ◦3 ^[3,22,70] |
| 30 | -12.90418 | ◦2 ^[3,27] | 63 | -34.71043 | ◦3 ^[1,13,48] | 96 | -61.45780 | ◦3 ^[2,25,69] |
| 31 | -13.45832 | ◦2 ^[3,28] | 64 | -35.70522 | ◦2 ^[14,49] | 97 | -62.23226 | ◦3 ^[2,24,70] |
| 32 | -14.06814 | ◦2 ^[4,28] | 65 | -36.52133 | ◦2 ^[13,51] | 98 | -63.19786 | ◦3 ^[3,25,70] |
| 33 | -14.65509 | ◦2 ^[4,29] | 66 | -37.26078 | ◦2 ^[12,53] | 99 | -63.80895 | ◦2 ^[28,70] |
| 34 | -15.26558 | ◦2 ^[4,30] | 67 | -37.97035 | ◦2 ^[15,51] | 100 | -64.84156 | ◦3 ^[4,26,70] |

of the optimal configurations will persist for N as large as several hundred. These expectations come from observing the convergence of the trap locations to their optimum configuration, which appear to be of familiar form, as well as results obtained by others for arrangements of several hundred confined particles [19,20,22].

V. CONCLUSIONS

In the current contribution, global optimization of configurations of N small traps minimizing the average mean first passage time (1.2) of a Brownian particle required to leave the unit sphere [see problem (1.1)] was performed. In Sec. II a simple exact solution (2.1) of the narrow capture problem (1.1) for a single trap, as well as the explicit approximate asymptotic solutions (2.2) for $N \geq 1$ small traps of size $\epsilon \ll 1$ derived in Ref. [24], were reviewed. The asymptotic solutions (2.2) involve a trap interaction term p_c (2.4), whose optimization is equivalent to the minimization of the AMFPT in the domain.

In Sec. III the asymptotic approximations were tested against the exact and numerical solutions under the conditions when the asymptotic assumptions were violated, in order to examine the accuracy of the asymptotic approximations throughout the domain, as well as test the relationship between the trap sizes and locations with the accuracy of the approximation. It was found that the asymptotic MFPT is remarkably accurate in regions of the domain not only relatively far from the surface of a trap, producing relative errors $\sim 10^{-7}$, but also near the trap, where the relative errors were $\lesssim 10^{-6}$ as close as $|x| \geq 2\epsilon$. Moreover, the average MFPT provided by the asymptotic formula (2.2b) was found accurate within 1% relative error even for rather large size of a single trap ($\epsilon \lesssim 0.2$), or for a pair of traps located close to each other (distances $\sim \epsilon$), or a trap located closely to the reflective domain boundary about (distances $\sim \epsilon$). From the analysis of the quality of asymptotic approximations of simple trap configurations, it was concluded that these approximations are acceptable for the study of optimal configurations of more complicated configurations of small traps.

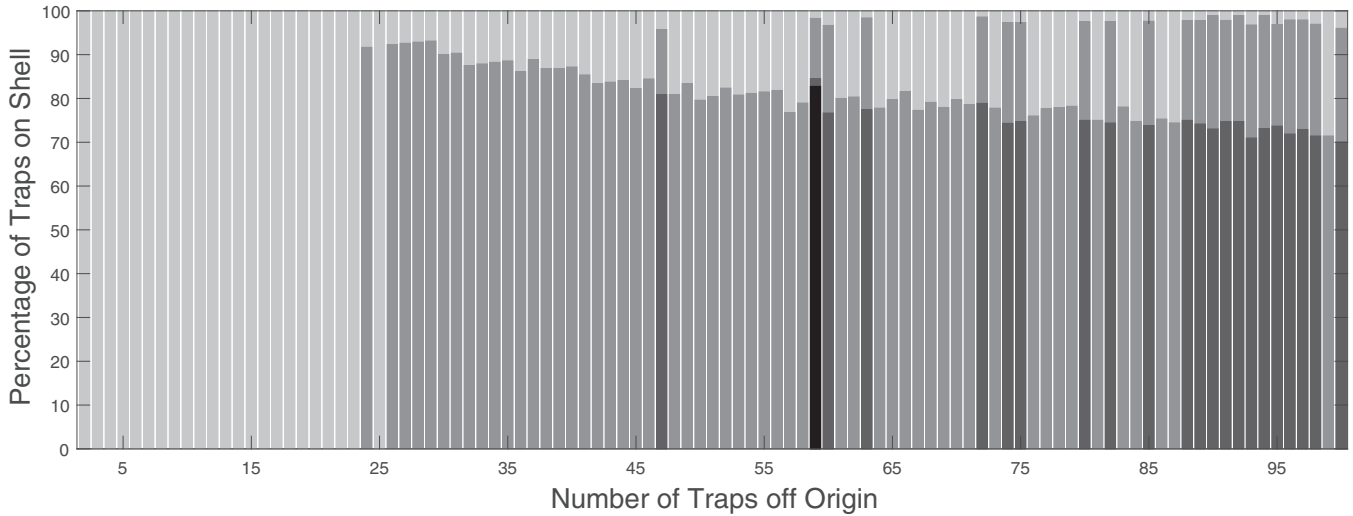


FIG. 14. The distribution of traps over each shell. The length of each bar represents the percentage of traps, relative to the total number of traps excluding the trap at the origin, which are located on a particular shell. For configurations where multiple shells exist, each shell is distinguished by the shading of the bar, the lightest shading corresponds to the innermost traps, and the darkest to the outermost.

Putative optimal global arrangements of $2 \leq N \leq 100$ traps minimizing the AMFPT in the unit sphere were sought in Sec. IV. It was found that the interaction energies p_c (2.4) of such configurations lie on a monotone decreasing curve. The radial distribution of traps in optimal configurations was examined, and it was found that the traps were distributed near, though not exactly on, surfaces of concentric spheres. It was found that, in general, the radii of these spheres grow larger as the number of traps found about them increases. A table of minimal interaction energies and radial trap distributions, were constructed (Table III; Figs. 14 and 15).

It was found that the optimal configurations of traps in the narrow capture problem have a structure which resembles other energy minimizing configurations of particles in three dimensions, for example, the sphere-packing problem, both theoretical [41] and experimentally realized [42].

As the number of traps N increases, one may expect that the shell structure observed here will eventually dissipate, and the traps will be distributed “homogeneously” throughout the domain. Indeed, the structure of an optimal configuration is determined by the tendency of the traps to repel from one another, as well as from trap “images” in the reflective boundary. Figures 14 and 15 demonstrate that as N increases, so do the number of shells and the shell radii. If this trend continues, the distance between traps on different shells will become comparable to the distance between traps on a shell, and the distance between traps on the outermost shell and the boundary will become comparable to the distance between a trap and its immediate neighbor, hence the shells will effectively disappear.

For the structure of the optimal trap configurations observed in the current work, one might expect that the optimal arrangement of identical traps within the highly

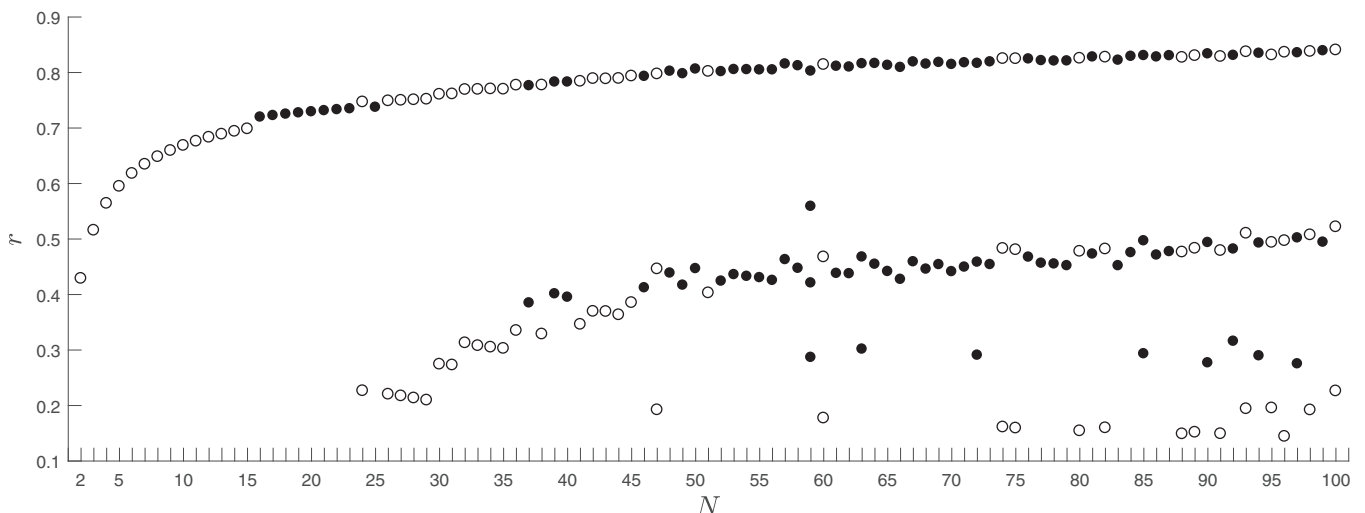


FIG. 15. The average radius of the traps associated with each shell vs the total number of traps. A filled marker indicates a trap at the origin, and an open marker indicates otherwise.

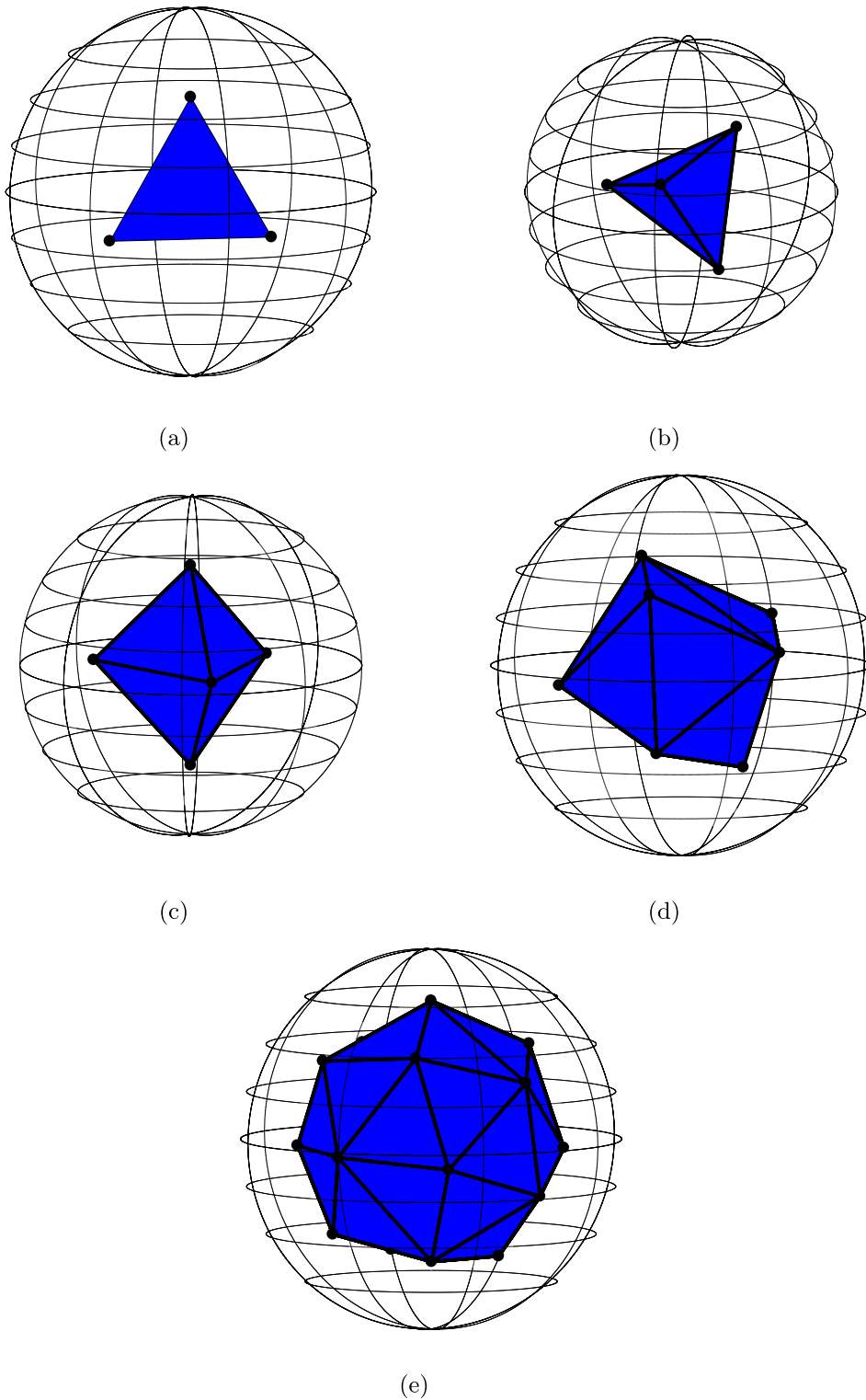


FIG. 16. Polyhedra with optimal trap locations as vertices for (a) $N = 3$, (b) $N = 4$, (c) $N = 5$, (d) $N = 8$, (e) $N = 19$. (The spherical shell structures for the optimal arrangements of $N = 5, 8, 19$ traps are shown in Figs. 10–12.)

symmetric domain of the unit sphere would be highly symmetric itself. Yet in the study of the optimal arrangement of confined particles, which is in essence the problem we consider here, symmetric configurations appear to arise only in special cases. Some examples of two-dimensional highly symmetric potential-minimizing arrangements can be found in Refs. [43,44], whereas in three dimensions, particles are often located about shells, such as spherical shells [19,20], or cylindrical shells [22] in the case of a cylindrically symmetric

container. Comparing our results with other optimal particle configurations in three-dimensional domains (see, e.g., Refs. [21,41,42,45]), it is not surprising to find that the traps lie *near* the surfaces of spheres rather than *on* them. For small N ($N < 24$), the traps lie on a single spherical shell, in particular, at the vertices of polyhedra, such as an equilateral triangle for $N = 3$, a tetrahedron for $N = 4$, and a trigonal bipyramid for $N = 5$ (Fig. 16); for the last, the distances from each of the traps at the north and south poles is slightly

smaller than that for traps in the equatorial plane (the same was observed in Ref. [45]).

An immediately accessible extension of the work done here is a study of configurations of nonidentical traps which minimize the average mean first-passage time; in particular, one may ask how capacitances (shape and size factors) of the traps (Table I) characterize and affect the N -trap configuration.

The asymptotic MFPT formulas (2.2) used in the current study involve the domain's Green's function which is known explicitly. It would be of interest and importance to generalize the expressions (2.2) to other domains (see a related work [40] for narrow escape problems). Moreover, when Green's functions which are not known in closed form, their approximations, such as those employed in Refs. [16,46], could be used. MFPT results in nonspherical domains would be useful, for example, to model intracellular interactions and chemical reactions in biological structures of irregular shapes, such as blood cells and dendrites. Direct numerical simulations for the problem (1.1) and their comparison of numerical simulations of Brownian motion confined to a reflecting domain containing absorbing traps is also of interest (similar work has been done for the narrow capture problem in two dimensions in Ref. [16]).

It is also interesting to study a possibility of deriving a scaling law that would predict a limiting behavior of the mean first-passage time, as the number N of "homogeneously"

distributed traps grows, $N \rightarrow \infty$, while the total volume (or another integral characteristic) of the trap set is controlled. This problem was successfully addressed, and linked with the dilute trap limit and a homogenized boundary value problem, in the model with boundary traps [27,29] (the narrow escape problem), but here it presents an additional difficulty, since the radial distribution of a large number of traps repelling according to the pairwise energy p_c (2.4) remains unknown. Another possible direction of future work could be to consider the case when the capture of a Brownian particle by the trap is imperfect, for example, time-dependent or probabilistic in nature (see, e.g., Ref. [47]).

Finally, while the putative globally optimal volume trap arrangements minimizing the AMFPT (2.2b) for the narrow capture problem (1.1) have been computed in the current work, no data exist about numbers or structure of local minima. Steps have been made to understand the structure of local minima of pairwise potential for surface-constrained problems (see, e.g., Ref. [36] and references therein), but little is understood about locally optimal arrangements of particles confined within three-dimensional domains.

ACKNOWLEDGMENT

A.C. is grateful to NSERC of Canada for research support through a Discovery grant RGPIN-2014-05733.

-
- [1] P. C. Bressloff, B. A. Earnshaw, and M. J. Ward, Diffusion of protein receptors on a cylindrical dendritic membrane with partially absorbing traps, *SIAM J. Appl. Math.* **68**, 1223 (2008).
 - [2] P. C. Bressloff and J. M. Newby, Stochastic models of intracellular transport, *Rev. Mod. Phys.* **85**, 135 (2013).
 - [3] G. Oshanin, O. Vasilyev, P. Krapivsky, and J. Klafter, Survival of an evasive prey, *Proc. Natl. Acad. Sci. USA* **106**, 13696 (2009).
 - [4] O. Bénichou, Y. Kafri, M. Sheinman, and R. Voituriez, Searching Fast for a Target on DNA Without Falling to Traps, *Phys. Rev. Lett.* **103**, 138102 (2009).
 - [5] R. Metzler, S. Redner, and G. Oshanin, *First-Passage Phenomena and Their Applications* (World Scientific, Singapore, 2014).
 - [6] D. Holcman and Z. Schuss, Escape through a small opening: Receptor trafficking in a synaptic membrane (unpublished).
 - [7] S. Redner, *A Guide to First-Passage Processes* (Cambridge University Press, Cambridge, 2001).
 - [8] Z. Zhang, B. Wu, H. Zhang, S. Zhou, J. Guan, and Z. Wang, Determining global mean-first-passage time of random walks on Vicsek fractals using eigenvalues of Laplacian matrices, *Phys. Rev. E* **81**, 031118 (2010).
 - [9] V. Tejedor, O. Bénichou, and R. Voituriez, Global mean first-passage times of random walks on complex networks, *Phys. Rev. E* **80**, 065104 (2009).
 - [10] M. Keldysh and L. Sedov, Effective solution of some boundary value problems for harmonic functions, *Dokl. Akad. Nauk SSSR* **16**, 7 (1937).
 - [11] M. Lavrentiev and B. Shabat, Methods of complex function theory (unpublished).
 - [12] M. S. Titcombe and M. J. Ward, An asymptotic study of oxygen transport from multiple capillaries to skeletal muscle tissue, *SIAM J. Appl. Math.* **60**, 1767 (2000).
 - [13] U. Seiferheld, H. Bässler, and B. Movaghar, Electric-Field-Dependent Charge-Carrier Trapping in a One-Dimensional Organic Solid, *Phys. Rev. Lett.* **51**, 813 (1983).
 - [14] A. Blumen and G. Zumofen, Energy transfer as a random walk on regular lattices, *J. Chem. Phys.* **75**, 892 (1981).
 - [15] A. E. Lindsay, A. J. Bernoff, and M. J. Ward, First passage statistics for the capture of a Brownian particle by a structured spherical target with multiple surface traps, *Multiscale Model. Simul.* **15**, 74 (2017).
 - [16] A. E. Lindsay, R. T. Spoonmore, and J. C. Tzou, Hybrid asymptotic-numerical approach for estimating first-passage-time densities of the two-dimensional narrow capture problem, *Phys. Rev. E* **94**, 042418 (2016).
 - [17] A. E. Lindsay, T. Kolokolnikov, and J. C. Tzou, Narrow escape problem with a mixed trap and the effect of orientation, *Phys. Rev. E* **91**, 032111 (2015).
 - [18] J. C. Tzou, S. Xie, and T. Kolokolnikov, First-passage times, mobile traps, and Hopf bifurcations, *Phys. Rev. E* **90**, 062138 (2014).
 - [19] S. L. Gilbert, J. J. Bollinger, and D. J. Wineland, Shell-Structure Phase of Magnetically Confined Strongly Coupled Plasmas, *Phys. Rev. Lett.* **60**, 2022 (1988).
 - [20] D. H. E. Dubin and T. M. O'Neil, Computer Simulation of Ion Clouds in a Penning Trap, *Phys. Rev. Lett.* **60**, 511 (1988).
 - [21] R. Rafac, J. P. Schiffer, J. S. Hangst, D. Dubin, and D. J. Wales, Stable configurations of confined cold ionic systems, *Proc. Natl. Acad. Sci. USA* **88**, 483 (1991).
 - [22] R. W. Hasse and J. Schiffer, The structure of the cylindrically confined Coulomb lattice, *Ann. Phys.* **203**, 419 (1990).
 - [23] R. F. Wuerker, H. Shelton, and R. Langmuir, Electrodynamical confinement of charged particles, *J. Appl. Phys.* **30**, 342 (1959).

- [24] A. F. Cheviakov and M. J. Ward, Optimizing the principal eigenvalue of the Laplacian in a sphere with interior traps, *Math. Comput. Model.* **53**, 1394 (2011).
- [25] T. Kolokolnikov, M. S. Titcombe, and M. J. Ward, Optimizing the fundamental Neumann eigenvalue for the Laplacian in a domain with small traps, *Eur. J. Appl. Math.* **16**, 161 (2005).
- [26] S. Pillay, M. J. Ward, A. Peirce, and T. Kolokolnikov, An asymptotic analysis of the mean first passage time for narrow escape problems: Part I: Two-dimensional domains, *Multiscale Model. Simul.* **8**, 803 (2010).
- [27] A. F. Cheviakov, M. J. Ward, and R. Straube, An asymptotic analysis of the mean first passage time for narrow escape problems: Part II: The sphere, *Multiscale Model. Simul.* **8**, 836 (2010).
- [28] A. F. Cheviakov, A. S. Reimer, and M. J. Ward, Mathematical modeling and numerical computation of narrow escape problems, *Phys. Rev. E* **85**, 021131 (2012).
- [29] A. F. Cheviakov and D. Zawada, Narrow-escape problem for the unit sphere: Homogenization limit, optimal arrangements of large numbers of traps, and the N^2 conjecture, *Phys. Rev. E* **87**, 042118 (2013).
- [30] S. Pillay, The narrow escape problem: A matched asymptotic expansion approach, Ph.D. thesis, University of British Columbia, 2008.
- [31] J. D. Pintér, LGO—A program system for continuous and Lipschitz global optimization, *Developments in Global Optimization* (Springer, Boston, MA, 1997), pp. 183–197.
- [32] T. Erber and G. Hockney, Complex systems: Equilibrium configurations of n equal charges on a sphere ($2 \leq n \leq 112$), *Adv. Chem. Phys.* **98**, 495 (1995).
- [33] D. Mehta, J. Chen, D. Z. Chen, H. Kusumaatmaja, and D. J. Wales, Kinetic Transition Networks for the Thomson Problem and Smale’s Seventh Problem, *Phys. Rev. Lett.* **117**, 028301 (2016).
- [34] B. Bergersen, D. Boal, and P. Palffy-Muhoray, Equilibrium configurations of particles on a sphere: The case of logarithmic interactions, *J. Phys. A* **27**, 2579 (1994).
- [35] T. Erber and G. Hockney, Comment on “Method of Constrained Global Optimization,” *Phys. Rev. Lett.* **74**, 1482 (1995).
- [36] W. J. M. Ridgway and A. F. Cheviakov, An iterative procedure for finding locally and globally optimal arrangements of particles on the unit sphere, *Comput. Phys. Commun.* **233**, 84 (2018).
- [37] N. N. Lebedev, *Worked Problems in Applied Mathematics* (Dover, New York, 2010).
- [38] E. M. Purcell and D. J. Morin, *Electricity and Magnetism* (Cambridge University Press, Cambridge, 2013).
- [39] J. Tzou, S. Xie, T. Kolokolnikov, and M. Ward, The stability and slow dynamics of localized spot patterns for the 3-D Schnakenberg reaction-diffusion model, *SIAM J. Appl. Dyn. Syst.* **16**, 294 (2017).
- [40] D. Gomez and A. F. Cheviakov, Asymptotic analysis of narrow escape problems in nonspherical three-dimensional domains, *Phys. Rev. E* **91**, 012137 (2015).
- [41] N. J. Sloane, R. H. Hardin, T. Duff, and J. H. Conway, Minimal-energy clusters of hard spheres, *Discrete Comput. Geom.* **14**, 237 (1995).
- [42] V. N. Manoharan, M. T. Elsesser, and D. J. Pine, Dense packing and symmetry in small clusters of microspheres, *Science* **301**, 483 (2003).
- [43] M. Saint Jean, C. Even, and C. Guthmann, Macroscopic 2D Wigner islands, *Europhys. Lett.* **55**, 45 (2001).
- [44] V. M. Bedanov and F. M. Peeters, Ordering and phase transitions of charged particles in a classical finite two-dimensional system, *Phys. Rev. B* **49**, 2667 (1994).
- [45] M. Hoare and P. Pal, Physical cluster mechanics: Statics and energy surfaces for monatomic systems, *Adv. Phys.* **20**, 161 (1971).
- [46] S. L. Marshall, A periodic Green’s function for calculation of Coulombic lattice potentials, *J. Phys.: Condens. Matter* **12**, 4575 (2000).
- [47] P. C. Bressloff and S. D. Lawley, Stochastically gated diffusion-limited reactions for a small target in a bounded domain, *Phys. Rev. E* **92**, 062117 (2015).